IOP Publishing Nanotechnology

Nanotechnology **32** (2020) 025709 (10pp) https://doi.org/10.1088/1361-6528/abbb4c

Why thermal conductivity of CaO is lower than that of CaS: a study from the perspective of phonon splitting of optical mode

Zhonghua Yang[1,2,4], Kunpeng Yuan[2,3,4], Jin Meng[1], Xiaoliang Zhang[3], Dawei Tang[3] and Ming Hu[2,5]

[1] School of Architecture and Civil Engineering, Shenyang University of Technology, Shenyang 110870, People's Republic of China
[2] Department of Mechanical Engineering, University of South Carolina, Columbia, SC 29201, United States of America
[3] Key Laboratory of Ocean Energy Utilization and Energy Conservation of Ministry of Education, School of Energy and Power Engineering, Dalian University of Technology, Dalian 116024, People's Republic of China

E-mail: hu@sc.edu

Received 11 July 2020, revised 11 September 2020
Accepted for publication 24 September 2020
Published 14 October 2020

Abstract

Generally speaking, for materials with the same structure, the thermal conductivity is higher for lighter atomic masses. However, we found that the thermal conductivity of CaO is lower than that of CaS, despite the lighter atomic mass of O than S. To uncover the underlying physical mechanisms, the thermal conductivity of CaM (M = O, S, Se, Te) and the corresponding response to strain is investigated by performing first-principles calculations along with the phonon Boltzmann transport equation. For unstrained system, the order of thermal conductivity is CaS > CaO > CaSe > CaTe. This order remains unchanged in the strain range of −2% to 5%. When the compressive strain is larger than 2%, the thermal conductivity of CaO surpasses that of CaS and becomes the highest thermal conductivity material among the four compounds. By analyzing the mode-dependent phonon properties, the phonon lifetime is found to be dominant over other influential factors and leads to the disparate response of thermal conductivity under strain. Moreover, the changing trend of three-phonon scattering phase space is consistent with that of phonon lifetime, which is directly correlated to the phonon frequency gap induced by the LO-TO splitting. The variation of Born effective charge is found to be opposite for CaM. The Born effective charge of CaO decreases with tensile strain increasing, demonstrating stronger charge delocalization and lower ionicity, while the Born effective charges of CaS, CaSe, and CaTe show a dramatic increase. Such variation indicates that the bonding nature can be effectively tuned by external strain, thus affecting the phonon anharmonic properties and thermal conductivity. The difference of bonding nature is further confirmed by the band structure. Our results show that the bonding nature of CaM can be modulated by external strain and leads to disparate strain dependent thermal conductivity.

Keywords: lattice thermal conductivity, first-principles, phonon anharmonicity, Boltzmann transport equation, mechanical strain, phonon lifetime, phonon transport

(Some figures may appear in colour only in the online journal)

[4] These authors contributed equally to this work.
[5] Author to whom any correspondence should be addressed.

1. Introduction

Heat transfer is one of the main forms of energy transfer in nature. Efficiently manipulating thermal transport in materials is one of the most appealing fundamental thermal physical problems, with two representatives but opposing aspects: on the one hand, increasing the thermal conductivity of the material to eliminate the heat accumulated performance of electronic equipment is essential to extend its lifetime [1–3]; on the other hand, reducing the thermal conductivity of the material is significant in the thermoelectricity and thermal insulation field [4–7]. As for the carriers of heat transfer, phonons play a dominant role in the thermal transport of semiconductors and insulators [8–11]. According to the phonon kinetic theory, the lattice thermal conductivity is a summation of contribution of all the phonon modes, given by [12, 13] $\kappa_\alpha = \sum_\lambda c_{ph,\lambda}\nu^2_{\alpha,\lambda}\tau_\lambda$, where κ_α denotes the lattice thermal conductivity along α direction in Cartesian coordinates, λ represents a phonon mode with wave vector **q** and phonon branch **s**, $\nu_{\alpha,\lambda}$ is the phonon group velocity of mode λ along α direction, τ_λ is the phonon lifetime of mode λ, and c_{ph} refers to the phonon volumetric specific heat of each mode. It is obvious that phonon transport in a material is governed by heat capacity, group velocity, and most importantly the phonon lifetime. In principle, the nature of the interatomic electrostatic interactions is the dominant factor to determine all these components mentioned above. Based on this concept, tremendous amounts of research efforts have been dedicated in the past decades to exploring robust ways to effectively modulate phonon transport. The external mechanical deformation is one of the most common and effective methods to manipulate thermal transport [14–19].

In recent years, alkaline earth chalcogenides (AM: A = Be, Mg, Ca, Sr, Ba; M = O, S, Se, Te) attracted tremendous research interests [20], including the theoretical and experimental research on them. This is because these compounds are thought to be promising in light-emitting diodes and laser diodes [21, 22]. Among them, CaM is the most widely used ranging from catalysis to microelectronics. A lot of studies using different *ab initio* methods have been performed on structural phase transitions, metallization, cohesive and elastic properties at ambient conditions and under high pressure on CaM [23–28]. However, the research of phonon transport in CaM is relatively rare. In order to seek thermoelectric materials with high conversion efficiency, Seko *et al* reported the first-principles calculation results of the thermal conductivity of CaM compounds [29]. The trend is CaS > CaO > CaSe > CaTe, but no physical mechanisms were analyzed further. Here, the strain is used to manipulate the thermal conductivity of CaO. Among the compounds formed by calcium and other elements of the oxygen family (CaO, CaS, CaSe, CaTe), due to the relatively light mass of CaO, it can be predicted that its thermal conductivity is relatively higher. However, the result unexpectedly shows that the thermal conductivity of CaO is lower than that of CaS, which aroused our great interest. Based on this, the first-principles approach is used to systematically study the thermal conductivity of CaO, CaS, CaSe, and CaTe. The underlying physical mechanism for the abnormal strain tuned thermal conductivity is also discussed from the perspective of bonding nature.

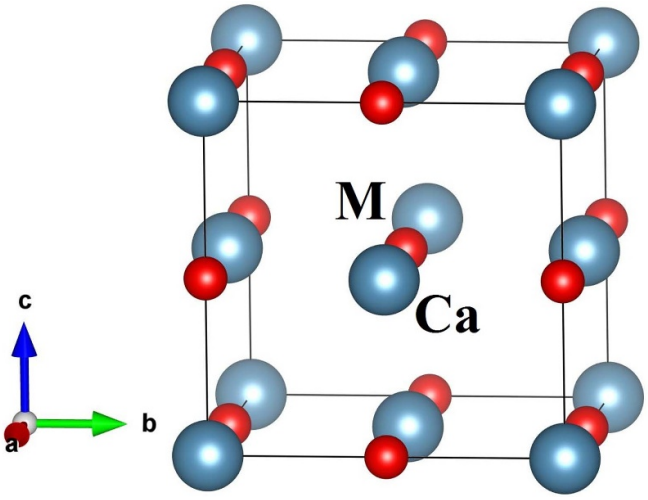

Figure 1. The conventional unit cell of CaM structure, where the blue and red atoms represent Ca and M (M = O, S, Se,Te).

2. Computational model and methods

All the first-principles calculations are based on density functional theory (DFT) as implemented in the Vienna *ab initio* simulation package (VASP) [30–32]. The Perdew-Burke-Ernzerhof (PBE) [33] of the generalized gradient approximation (GGA) is chosen as the exchange-correlation functional. The kinetic energy cutoff of the wave functions is set as 600 eV, and a Monkhorst-Pack [34] k-mesh of $6 \times 6 \times 6$ is used to sample the Brillouin Zone (BZ). The structures are allowed to be fully relaxed until both the energy convergence criteria of 10^{-8} eV and the force convergence threshold of 10^{-6} eV $\mathring{A}^{-1}$ are satisfied.

CaM (M = O, S, Se, Te) belong to the cubic crystal system with space group $Fm\bar{3}m$ (space group number: 225). The atomic coordinates of CaM crystals are Ca (0, 0, 0) and M (0.5, 0.5, 0.5), respectively (see figure 1). The fully relaxed lattice constant of bulk CaO is 4.838 Å, in good agreement with experimental value of 4.811 Å [27]. Due to the increase of atomic radius, the lattice constants of CaS, CaSe, and CaTe are monotonically increased to 5.718 Å, 5.965 Å, and 6.400 Å, respectively, which is quite normal and consistent with general knowledge. Tensile and compressive strains are applied by stretching and compressing the unstrained lattice constant a_0 by a certain percentage $\varepsilon = (a—a_0)/a_0$, where a is the lattice constant of strained structures. During the optimization, only the atomic positions are changed, with the lattice constant kept fixed.

The lattice thermal conductivity (κ_l) is obtained by iteratively solving the linearized Boltzmann-Peierls transport equation (BTE) as implemented in the ShengBTE package [35],

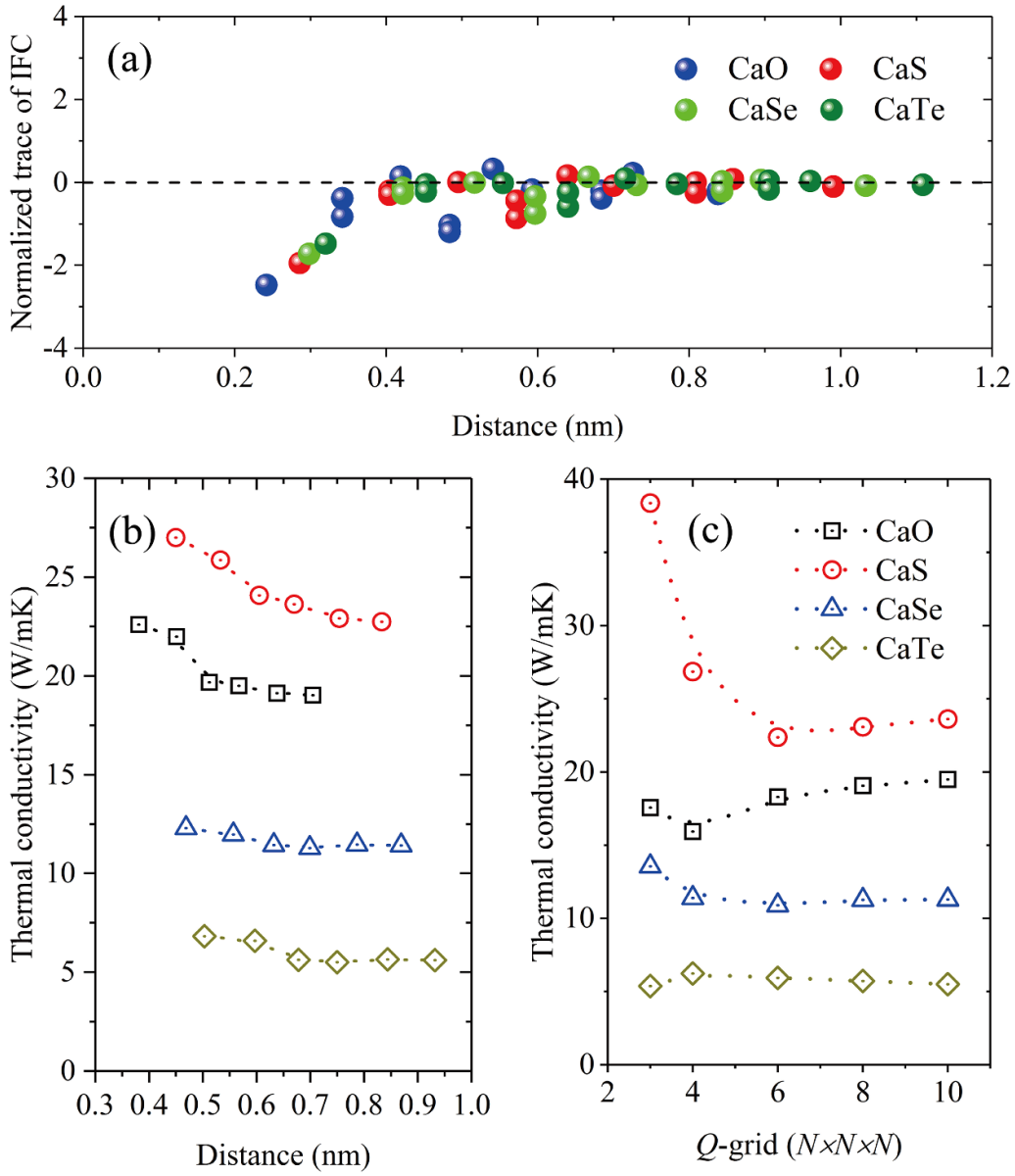

Figure 2. (a) Normalized trace of interatomic force constant tensors versus atomic distances. (b) Convergence test of thermal conductivity with respect to cutoff distance. (c) Convergence test of thermal conductivity with respect to Q-grid in phonon BTE calculation.

which only requires the inputs of second-order harmonic and third-order anharmonic interatomic force constants (IFCs) without any other adjustable parameters. A $2 \times 2 \times 2$ supercell and the Monkhorst–Pack k-mesh of $2 \times 2 \times 2$ are chosen to calculate the harmonic and anharmonic IFCs. The second-order harmonic IFCs are used to determine the phonon frequency and phonon eigenvector using the Phonopy code[36]. The anharmonicity is described using the third-order IFCs, while the contributions of the fourth and higher-order terms are neglected. The third-order IFCs can be evaluated based on the third-order derivatives of the total energy with respect to the atomic displacements. With the anharmonic IFCs, the scattering matrix can be constructed, based on which one can calculate all the three phonon scattering rates and then obtain the phonon lifetime. This anharmonic lattice dynamics method coupled with BTE has been widely used to study phonon transport in crystalline materials recently [37–46]. In addition, the Born effective charge (Z) and dielectric constant (ε) are obtained based on density functional perturbation theory (DFPT).

3. Simulation result and discussion

3.1. Lattice thermal conductivity

In the condition of considering the phonon-phonon scattering as determined by phonon anharmonicity, the lattice thermal conductivities (κ_l) of CaM (M = O, S, Se, Te) are obtained by solving the phonon BTE. The thermal conductivity convergence of CaM with respect to the cutoff radius and Q-grid are fully examined in figure 2. The convergence of cutoff radius of anharmonic IFCs should be tested firstly, because the cutoff

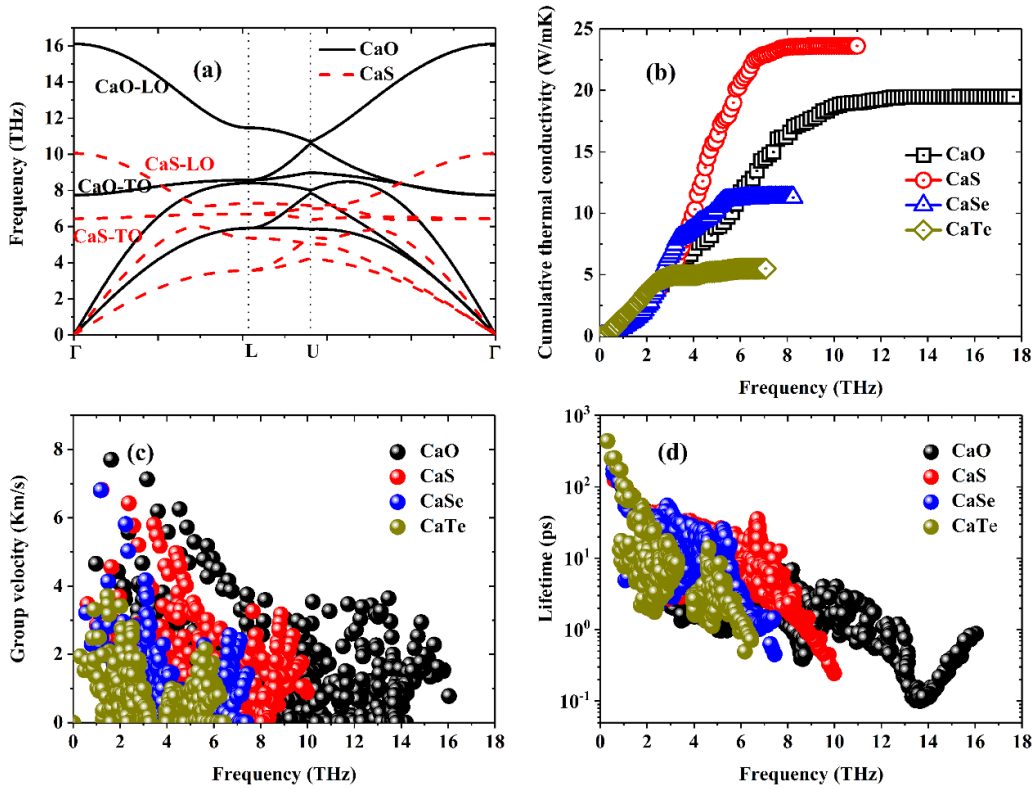

Figure 3. (a) The phonon dispersion of CaO and CaS. (b) The cumulative thermal conductivity of CaM with respect to frequency. (c) The frequency dependent group velocity of CaM. (d) The mode lifetime of CaM.

radius can be directly determined to get satisfactory thermal conductivity results based on the analysis of harmonic IFCs [47]. In order to quantify the strength of interatomic interactions which are described by harmonic IFCs, we calculated the normalized trace of interatomic force constant tensors [48]. According to this parameter, one can directly determine how large the cutoff radius should be used to evaluate the anharmonic IFCs by effectively including the possibly strong interaction strength as revealed by the large trace value. Figure 2(a) is the normalized trace of IFC in CaM, it is clear that when the cutoff radius is less than 0.512 nm (blue ball), 0.605 nm (red ball), 0.632 nm (green ball) and 0.678 nm (olive ball), which are corresponding to fourth-nearest neighbors of CaM (M = O, S, Se, Te) respectively, there exist strong interactions between Ca and M atoms. When the cutoff radius is bigger than the threshold value (fourth-nearest neighbor), the trace values are very weak, indicating negligible force constants. Similar conclusions can also be obtained by the convergence test of CaM thermal conductivity in figure 2(b). Before the cutoff radius achieving the threshold value, the CaM thermal conductivities drop dramatically, and the thermal conductivities converge quickly up to the fourth-nearest neighbors, which confirms the evaluation from the strength of the harmonic IFCs in figure 1(a). It is also shown in figure 2(c) that the thermal conductivities of CaM possess a well-converged behavior when Q-grid is greater than $6 \times 6 \times 6$. Therefore, considering both computational cost and accuracy, the interactions are truncated up to the fifth-nearest neighbors and Q-grid is set as $10 \times 10 \times 10$ for the following anharmonic IFCs calculations.

Phonon dispersion is crucial for the calculation of phonon transport properties. By using finite displacement difference method, we obtained the harmonic IFCs and hence the phonon dispersion relations of CaM. To accurately predict the phonon frequencies for polar materials, the effects of dipole-dipole interactions are incorporated into the dynamic matrix based on the Born effective charges and high-frequency dielectric constants, which can result in the splitting between longitudinal and transverse optical (LO-TO) phonon frequencies presented at the Γ point. Due to the similarity, only phonon dispersion curves of CaO and CaS along the high symmetry path are shown in figure 3(a). It is obvious that all phonon modes of CaS experience a downward shift in frequency as compared with CaO. In fact, as the atomic mass of the compound increases, the phonon frequency of CaM (M = O, S, Se, Te) will decrease substantially. Moreover, there is a large LO-TO splitting in the vicinity of Γ point. In the three-phonon scattering process, both energy and momentum conservation should be satisfied. The phonon splitting between LO and TO will open a frequency gap and largely affect the available three-phonon scattering channels. We will perform a detailed analysis about the effect of LO-TO splitting on the thermal conductivity in the following text.

In figure 3(b), the cumulative thermal conductivities of CaM are compared, from which we can quantify the contributions of different phonon frequencies to lattice thermal conductivity. In the frequency range of 0–2 THz, the thermal conductivity of CaTe is relatively higher, then the thermal conductivity of CaS increases significantly when the

phonon frequency is above 2 THz. Although the phonon modes with frequency larger than 10 THz still contribute to the thermal conductivity of CaO, CaS has the highest thermal conductivity among the four materials. The room-temperature thermal conductivities of the four compounds are 19.50 W mK^{-1} (CaO), 23.63 W mK^{-1} (CaS), 11.29 W mK^{-1} (CaSe), and 5.50 W mK^{-1} (CaTe), respectively. They are consistent with the theoretical results using first-principles anharmonic lattice-dynamics calculations [29]. It is worth noting that the thermal conductivity of CaO is lower than that of CaS, which is opposite to the general trend that those with heavier elements have lower thermal conductivity for crystals with the same structure [49, 50]. To elucidate the physical mechanism behind this phenomenon, the mode-level phonon group velocity and phonon lifetime are calculated and analyzed in detail.

From the phonon group velocity shown in figure 3(c), we can see that the group velocity increases with the decrease of the atomic mass of CaM. As we all know, the phonon group velocity is given by the slope of the dispersion relations $v = \partial\omega/\partial q$. From the phonon dispersion in figure 3(a), it can be seen that the group velocity of CaO is larger than that of CaS, which is evidenced by the highly dispersive acoustic phonon branches in the vicinity of Γ point. Obviously, the phonon group velocity cannot explain the abnormal lower thermal conductivity of CaO than that of CaS.

Apart from the phonon group velocity, the phonon lifetime is another key factor determining thermal conductivity. Figure 3(d) shows the frequency-dependent phonon lifetimes of CaM. It is found that the phonon lifetime of CaTe is higher in the range of 0–2 THz. Meanwhile, the phonon lifetime of CaS becomes the largest in the high frequency range (4–7 THz). This variation trend of the phonon lifetime is consistent with the results of the cumulative thermal conductivity in figure 3(b). Combining the results of phonon group velocity and phonon lifetime, we can conclude that phonon lifetime is the dominant factor for the counterintuitive phenomenon that the thermal conductivity of CaS with heavier atomic mass is larger than that of CaO.

3.2. *Strain tuned lattice thermal conductivity*

Through the above analysis, it can be clear that the phonon anharmonic scattering is the main factor determining the thermal conductivity of CaM. As is known to everyone, materials need to be used in different environments, compression and tension are important parameters to material thermodynamic properties, it can be used as an effective method to manipulate the thermal conductivity of materials. Based on this, we investigate the response of thermal conductivity to external strains. The thermal conductivity of CaM at different applied strains are shown in figure 4. When the applied strain changes from 5% (tensile) to −5% (compressive), the thermal conductivity of CaM increases monotonically. In the interval of −1% and 5% strain, the order of thermal conductivity is CaS > CaO > CaSe > CaTe. When the compressive strain reaches −2%, CaO has the highest thermal conductivity among the four materials, and the order of thermal conductivity remains with the further increase of compressive strain.

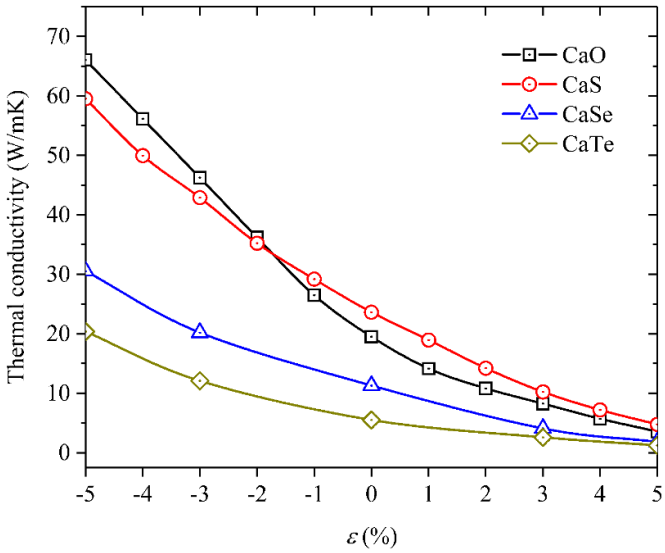

Figure 4. The thermal conductivity of CaM (M = O, S, Se, Te) under tensile ($\varepsilon > 0$) and compressive ($\varepsilon < 0$) strain.

The anharmonic phonon parameters are shown in figure 5. Figure 5(a) compares the phonon lifetimes of CaO and CaS at some representative strains. It is clearly seen that the phonon lifetime of CaO decreases significantly when strain changes from −5% (compressive strain) to 5% (tensile strain). Interestingly, when the strain is compressive, there is slight difference in phonon lifetime for CaS. However, for CaS under tensile strain, more significant reduction in phonon lifetime is observed.

For further insight into the anharmonic interactions, the Grüneisen parameter and scattering phase space are computed, which are used to characterize the scattering strength and the number of available phonon scattering channels. We found that the magnitude of the Grüneisen parameter of both materials is enchanced greatly when tensile strain is applied. In contrast, the Grüneisen parameter of both materials almost does not change with compressive strain. It is known that the larger the Grüneisen parameter, the stronger the anharmonicity. The larger Grüneisen parameter at high tensile strains leads to lower thermal conductivity, however, the almost unchanged Grüneisen parameter cannot explain the large variation in thermal conductivity of CaO under compressive strains.

To further understand the disparate strain dependent phonon lifetime of CaO and CaS, the three-phonon scattering phase space is calculated. This phase space is determined by integrating over delta functions that represent the conservation of energy and crystal momentum conditions [51]:

$$\omega_j(\mathrm{q}) \pm \omega_{j'}(\mathrm{q}') = \omega_{j''}(\mathrm{q}''), \quad \mathrm{q} \pm \mathrm{q}' = \mathrm{q}'' + \mathrm{G} \qquad (1)$$

where $\omega_j(\mathrm{q})$ is the phonon frequency of mode (j, q), and j,q are each phonon branch and momenta of phonon, respectively. G is a reciprocal lattice vector which is zero for Normal processes and non-zero lattice vector for Umklapp processes. ±signs correspond to the two types of possible three-phonon processes [52]. Equation (1) imposes severe constraints on the phase space available for three-phonon scattering.

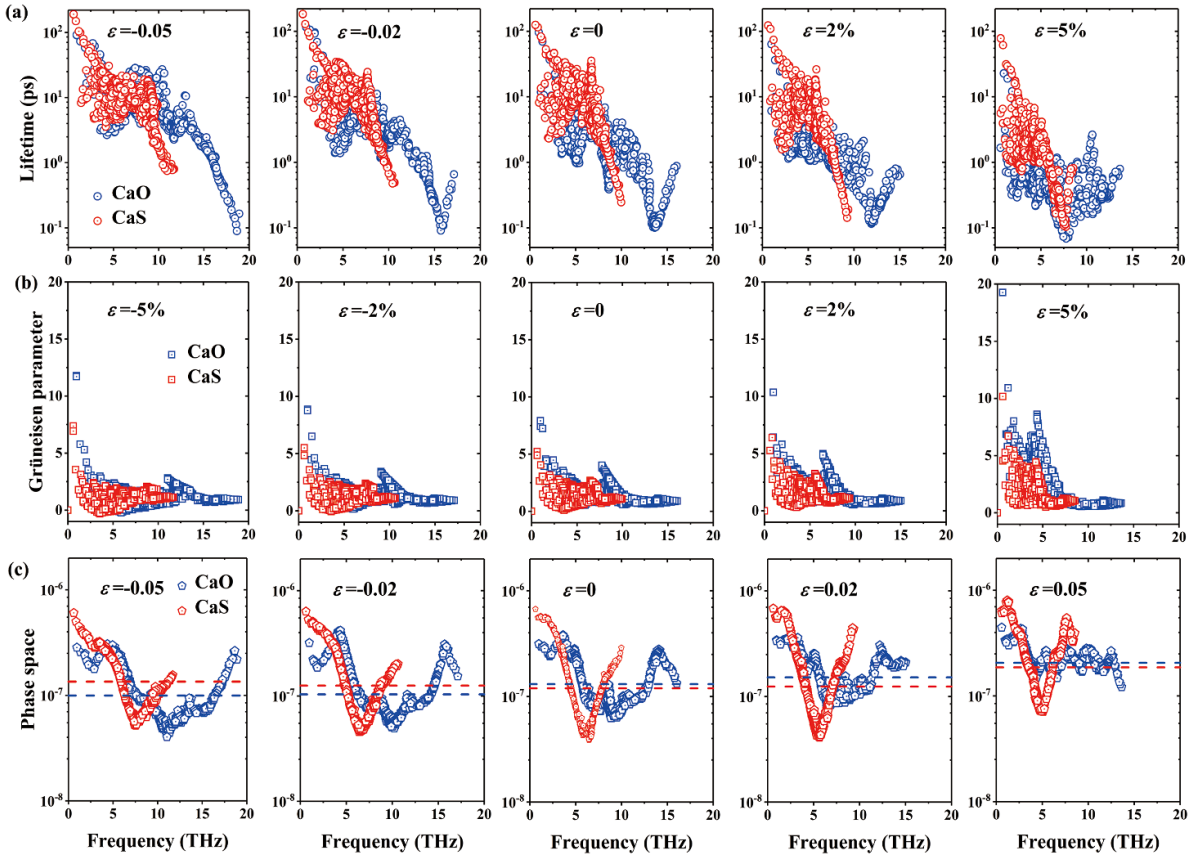

Figure 5. (a) The phonon lifetime of CaO and CaS under compressive and tensile strain. (b) The Grüneisen parameter of CaO and CaS under different strain. (c) The phase space of CaO and CaS under different strain. The blue and red dashed lines are the average phase space value of CaO and CaS, respectively.

To explore and clarify the mechanism behind, the three-phonon scattering phase space (P_3) is calculated as [35–53]:

$$P_3 = \frac{2}{3\Omega}\left(P_3^{(+)} + \frac{1}{2}P_3^{(-)}\right) \tag{2}$$

where

$$P_3^{(\pm)} = \sum_j \int dq D_j^{(\pm)}(q) \tag{3}$$

and

$$D_j^{(\pm)}(q) = \sum_{j',j''} \int dq' \delta\left(\omega_j(q) \pm \omega_{j'}(q') - \omega_{j''}(q \pm q'' - G)\right) \tag{4}$$

where Ω is a normalization factor. In equation (3) and (4), $D_j^{(\pm)}(q)$ is the two phonon density of states and momentum conservation has already been imposed on q'' [54]. According to equations (2)–(4), P_3 contains a large amount of scattering events that satisfy the conservation conditions and can be used to assess quantitatively the number of scattering channels available for each phonon mode. Consequently, there is an inverse relationship between P_3 and the intrinsic lattice thermal conductivity of a material [55].

In figure 5(c), the dash lines are the average phase space of CaO and CaS which are showed by scatter plots. According to this parameter, one can directly recognize how the scattering phase space is changing with strain in CaO and CaS. For CaO, the scattering phase space experiences an upward shift when the applied strain is changed from compressive to tensile. Especially, starting from -2%, the phase space rises rapidly in the frequency range of 7 THz $\sim$ 10 THz. As for CaS, there is no obvious change in the phase space until the strain is larger than 2%, so that the average value of CaS phase space begins to be lower than that of CaO in the strain range of -2% to 0%. These results are consistent with the strain-dependent phonon lifetime of CaO and CaS. Therefore, considering the results of Grüneisen parameter and scattering phase space, we can conclude that the scattering phase space is the governing factor that determining the phonon lifetime under strains.

3.3. *Insight from phonon splitting of optical modes*

It has been clear that the phase space leads to the disparate strain dependent phonon lifetime of CaO and CaS. More specifically, the increased phase space mainly comes from the high-frequency phonon modes which belong to optical branches. As we know, the scattering phase space is determined by the energy conservation and momentum conservation

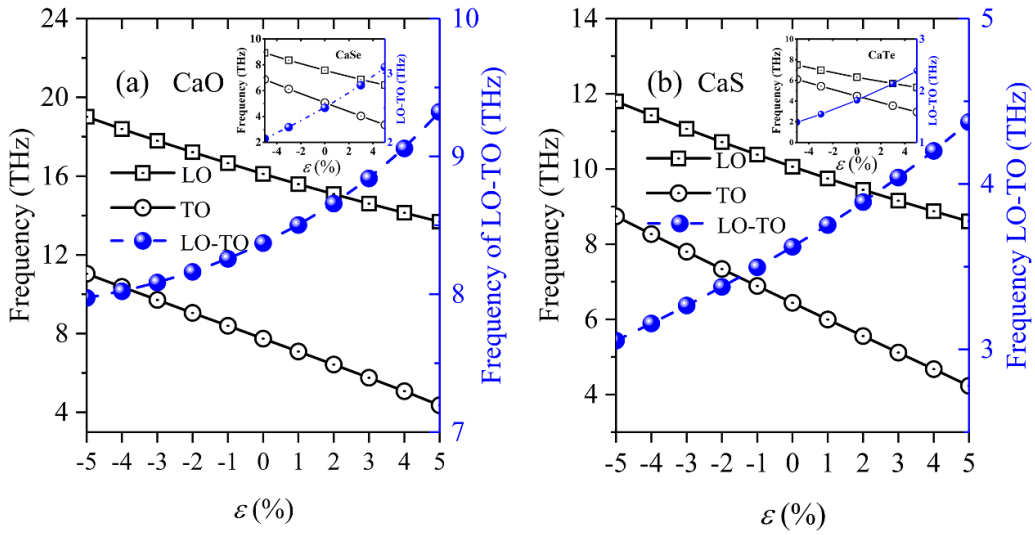

Figure 6. The splitting degrees of CaM optical phonon mode under tensile ($\varepsilon > 0$) and compressive ($\varepsilon < 0$) strain. (a) CaO, (inset) CaSe. (b) CaS (inset) CaTe.

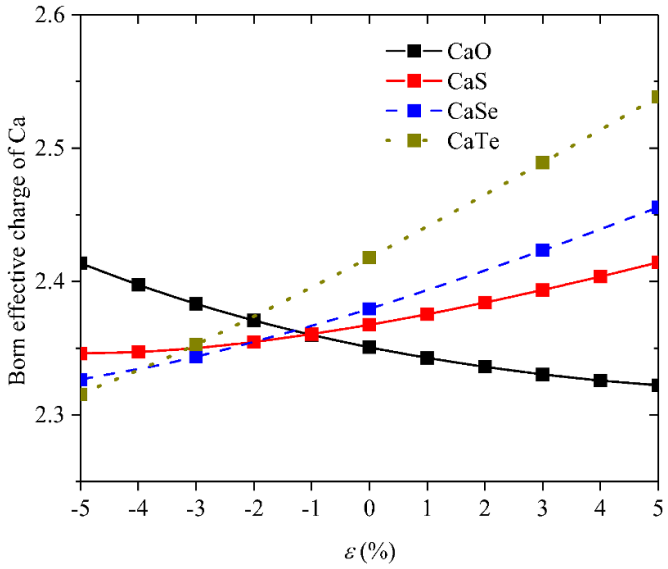

Figure 7. The strain dependent Born effective charge of CaM (M = O, S, Se, Te), where CaO shows distinctly different behavior where the Born effective charge decreases when external strain changes from compressive ($\varepsilon < 0$) to tensile ($\varepsilon > 0$) strain.

of three involved phonons. As Lindsay *et al* suggested [56], three-phonon scattering processes involving optical phonons will increase and contribute significantly to thermal resistance for materials with large LO-TO splitting. Therefore, the difference of LO-TO splitting in CaO and CaS will result in different response of phonon lifetime to external strain.

Here, the splitting degrees of optical phonon modes at Γ point are shown in figure 6. Among the curves, the red line represents the LO branch, the green line represents the TO branch, and the blue line represents the frequency gap between LO and TO. From compressive to tensile strain, the phonon frequencies of LO and TO branches decrease linearly. The frequency gap induced by the LO-TO splitting increases with the increase of tensile strain. For CaO, the frequency gap changes from 8 THz at −5% (compressive strain) to 9.3 THz at +5% (tensile strain). The magnitude of frequency gap change for CaS is about 1.3 THz, similar to CaO, but only changed from 3 THz to 4.3 THz. As discussed above, the scattering phase space of CaO increases gradually when the applied strain changes from compressive to tensile, while the scattering phase space of CaS does not show obvious change until the strain is larger than 2% which corresponds to the LO-TO splitting of CaS at 4 THz. Based on the LO-TO splitting effects on phonon scattering process, so it is reasonable to believe that, for CaS, there could be a much enhancement in scattering phase space when the LO-TO splitting is larger than 4 THz.

It is well known that LO-TO splitting is related to the long-range Coulomb interactions which partly depends on the Born effective charge. Moreover, Born effective charge characterizes the charge redistribution of chemical compound and indicates the bond ionicity, which are directly correlated to the thermal transport properties [57]. In figure 7, we present the Born effective charge of Ca ion. It can be seen that the Born effective charge of CaO decreases with the increase of tensile strain, which is fundamentally different from other CaM. In addition, the variation of Born effective charge for CaO is greatly less than that of other CaM. These results agree well with previous study by first-principles calculations [58]. When the strain changes from compressive to tensile, the Born effective charge of CaO is closer to the nominal charge of Ca ions, indicating stronger charge delocalization and lower ionicity, while the Born effective charge of CaS is further away from the nominal charge of Ca ions, the bond ionicity of CaS, CaSe, and CaTe is greater than that of CaO, thus the charge is localized on the ions.

Furthermore, in figure 8, we show the band structures of CaO and CaS under compressive and tensile strains, respectively. CaO and CaS are insulators with direct band gap no matter the applied strain is compressive or tensile. For CaO, the band gap decreases from 3.549 eV to 3.497 eV when

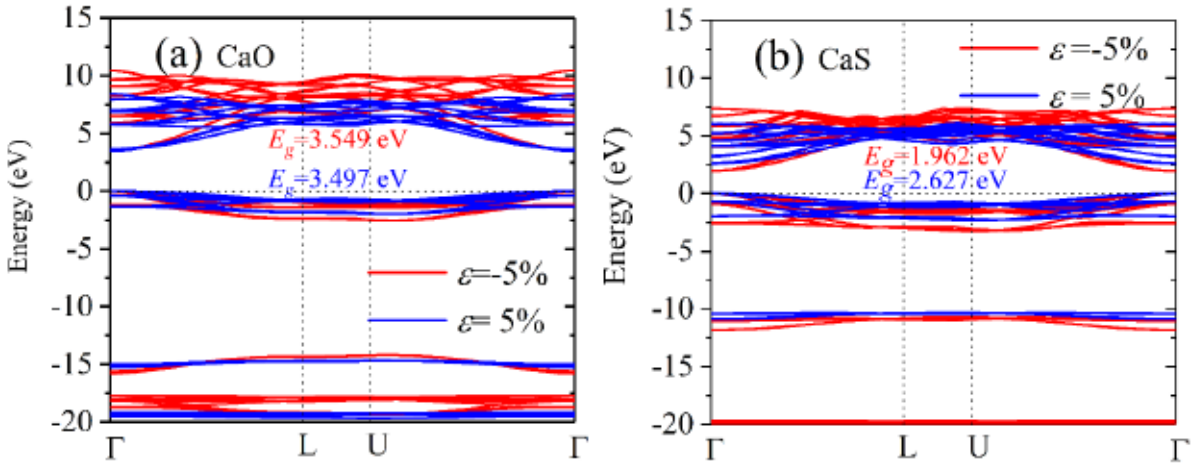

Figure 8. Band structure of (a) CaO and (b) CaS under compressive (5%) and tensile (5%) strains.

the stain changes from −5% to 5%, which is an indication of charge delocalization. However, for CaS, the conduction band moves towards high-energy region when the tensile strain is applied, the band gap becomes wider from 1.962 eV to 2.627 eV, showing stronger charge localization. The change of band gap with strain is consistent with the results of Born effective charge, demonstrating that the bond ionicity of CaO is different from CaS, CaSe, and CaTe. Therefore, it is reasonable to conclude that the disparate variation of bond ionicity of CaM with applied strain has a strong influence on the phonon splitting and phonon anharmonicity, and thus affects the lattice thermal conductivity of CaM.

4. Conclusion

In summary, first-principles calculations combined with phonon Boltzmann transport equation is performed to systematically study the lattice thermal conductivity of CaM (M = O, S, Se, Te) and its response to external mechanical strain. For the unstrained system, the thermal conductivity of CaO is much lower than that of CaS despite the light atomic mass of CaO. When tensile strain is applied, the thermal conductivity of CaM decreases and CaS has the highest thermal conductivity among the four compounds. As compressive strain increases, the thermal conductivity of CaO exhibits a dramatic increase and is higher than CaS when the compressive strain is larger than 2%. The analysis of phonon related properties reveals that the disparate strain tuned thermal conductivity of CaM is rooted in the phonon anharmonicity stemming from the different bonding nature among CaM. Due to the increase of frequency gap induced by LO-TO splitting, three-phonon scattering phase space of CaO increases gradually in the strain range of −5% ∼ 5%. In contrast, although the LO-TO splitting is also enhanced, three-phonon scattering phase space of CaS is not much sensitive to stretching and compressing until the tensile strain increases up to 2%. Further analysis shows the Born effective charge of Ca ion in CaO is closer to the nominal charge of Ca ions when the strain changes from compressive to tensile, which is opposite to the variation of other CaM structures, indicating stronger charge delocalization and lower ionicity. It is further verified by the decrease of the band gap of CaO when stretching the structure. The results obtained in this work provide a comprehensive understanding of the intrinsic thermal transport of CaM lattices and pave the way for manipulating phonon transport in other crystalline materials, especially ionic crystals.

Acknowledgments

This project is supported by the fund of Natural Science Foundation of Liaoning Province, China (Grant Nos. 20180540122, 200005636, 200005720). K Y acknowledges the support from the China Scholarship Council. X Z and D T acknowledge the support from the National Natural Science Foundation of China [51720105007 and 51806031], the Fundamental Research Funds for the Central Universities [DUT16RC(3)116]. Research reported in this publication was supported in part by the National Science Foundation (Award Number 1905775) and SC EPSCoR/IDeA Program under NSF OIA-1655740 via SC EPSCoR/IDeA 20-SA05.

ORCID ID

Ming Hu https://orcid.org/0000-0002-8209-0139

References

[1] Kang J S, Li M, Wu H, Nguyen H and Hu Y 2018 Experimental observation of high thermal conductivity in boron arsenide *Science* **361** 575
[2] Tian F *et al* 2018 Unusual high thermal conductivity in boron arsenide bulk crystals *Science* **361** 582
[3] Li S, Zheng Q, Lv Y, Liu X, Wang X, Huang P Y, Cahill D G and Lv B 2018 High thermal conductivity in cubic boron arsenide crystals *Science* **361** 579
[4] Islam A S M J, Islam M S, Ferdous N, Park J, Bhuiyan A G and Hashimoto A 2019 Anomalous temperature dependent thermal conductivity of two-dimensional silicon carbide *Nanotechnology* **30** 445707

[5] Wu X and Han Q 2020 Thermal conductivity of defective graphene: an efficient molecular dynamics study based on graphics processing units *Nanotechnology* **31** 215708

[6] Mukhopadhyay S, Parker D S, Sales B C, Puretzky A A, McGuire M A and Lindsay L 2018 Two-channel model for ultralow thermal conductivity of crystalline Tl_3VSe_4 *Science* **360** 1455

[7] Xia Y, Pal K, He J, Ozoliņš V and Wolverton C 2020 Particlelike phonon propagation dominates ultralow lattice thermal conductivity in crystalline Tl_3VSe_4 *Phys. Rev. Lett.* **124** 065901

[8] Qin G, Qin Z, Yue S, Yan Q-B and Hu M 2017 External electric field driving the ultra-low thermal conductivity of silicene *Nanoscale* **9** 7227–34

[9] Yin Y, Li D, Hu Y, Ding G, Zhou H and Zhang G 2020 Phonon stability and phonon transport of graphene-like borophene *Nanotechnology* **31** 315709

[10] Liu C, Yang J, Xi J and Ke X 2019 The origin of intrinsic charge transport for Dirac carbon sheet materials: roles of acetylenic linkage and electron–phonon couplings *Nanoscale* **11** 10828–37

[11] Yang X, Feng T, Li J and Ruan X 2019 Stronger role of four-phonon scattering than three-phonon scattering in thermal conductivity of III–V semiconductors at room temperature *Phys. Rev.* B **100** 245203

[12] Bao H, Chen J, Gu X and Cao B 2018 A review of simulation methods in micro/ nanoscale heat conduction *ES Energy Environ.* **16** 16–55

[13] Shafique A and Shin Y-H 2020 The effect of non-analytical corrections on the phononic thermal transport in InX (X = S, Se, Te) monolayers *Sci. Rep.* **10** 1093

[14] Yuan K, Zhang X, Li L and Tang D 2019 Effects of tensile strain and finite size on thermal conductivity in monolayer WSe2 *Phys. Chem. Chem. Phys.* **21** 468–77

[15] Wang H, Li Q, Gao Y, Miao F, Zhou X-F and Wan X G 2016 Strain effects on borophene: ideal strength, negative Possion's ratio and phonon instability *New J. Phys.* **18** 073016

[16] Wang F Q, Hu M and Wang Q 2019 Ultrahigh thermal conductivity of carbon allotropes with correlations with the scaled Pugh ratio *J. Mater. Chem.* A **7** 6259–66

[17] Xiao R C, Shao D F, Lu W J, Lv H Y, Li J Y and Sun Y P 2016 Enhanced superconductivity by strain and carrier-doping in borophene: a first principles prediction *Appl. Phys. Lett.* **109** 122604

[18] Dheeraj K V S, Kannam S K and Sathian S P 2020 Thermal conductivity of graphene under biaxial strain: an analysis of spectral phonon properties *Nanotechnology* **31** 345703

[19] Yang Z, Yuan K, Meng J and Hu M 2020 Electric field tuned anisotropic to isotropic thermal transport transition in monolayer borophene without alternating atomic structures *Nanoscale* **12** 19178–90

[20] Arya B, Aynyas M and Sanyal S 2008 High pressure study of structural and elastic properties of barium chalcogenides *Indian J. Pure Appl. Phys.* **46** 722–6

[21] Haase M A, Qiu J, DePuydt J M and Cheng H 1991 Blue-green laser diodes *Appl. Phys. Lett.* **59** 1272–4

[22] Heng K L, Chua S J and Wu P 2000 Prediction of semiconductor material properties by the properties of their constituent chemical elements *Chem. Mater.* **12** 1648–53

[23] Abdus Salam M M 2018 Theoretical study of CaO, CaS and CaSe via first-principles calculations *Results Phys.* **10** 934–45

[24] Fan Q, Chai C, Wei Q, Yang Y, Qiao L, Zhao Y, Zhou P, Xing M, Zhang J and Yao R 2015 Mechanical and electronic properties of Ca1 xMgxO alloys *Mater. Sci. Semicond. Process.* **40** 676–84

[25] Raty J-Y, Schumacher M, Golub P, Deringer V L, Gatti C, Wuttig M and Quantum-Mechanical A 2019 Map for bonding and properties in solids *Adv. Mater.* **31** 1806280

[26] Deng Y, Jia O-H, Chen X-R and Zhu J 2007 Phase transition and elastic constants of CaO from first-principle calculations *Physica* B **392** 229–32

[27] Albuquerque E L and Vasconcelos M S 2008 Structural, electronics and optical properties of CaO *J. Phys.: Conf. Ser.* **100** 042006

[28] Yan J and Zhao C Y 2014 First-principle study of CaO/Ca(OH)2 thermochemical energy storage system by Li or Mg cation doping *Chem. Eng. Sci.* **117** 293–300

[29] Seko A, Togo A, Hayashi H, Tsuda K, Chaput L and Tanaka I 2015 Prediction of low-thermal-conductivity compounds with first-principles anharmonic lattice-dynamics calculations and Bayesian optimization *Phys. Rev. Lett.* **115** 205901

[30] Kresse G and Furthmüller J 1996 Efficiency of ab-initio total energy calculations for metals and semiconductors using a plane-wave basis set *Comput. Mater. Sci.* **6** 15–50

[31] Kresse G and Furthmüller J 1996 Efficient iterative schemes for ab initio total-energy calculations using a plane-wave basis set *Phys. Rev.* B **54** 11169–86

[32] Kresse G and Joubert D 1999 From ultrasoft pseudopotentials to the projector augmented-wave method *Phys. Rev.* B **59** 1758–75

[33] Perdew J P, Burke K and Ernzerhof M 1996 Generalized gradient approximation made simple *Phys. Rev. Lett.* **77** 3865–8

[34] Monkhorst H J and Pack J D 1976 Special points for Brillouin-zone integrations *Phys. Rev.* B **13** 5188–92

[35] Li W, Carrete J, Katcho A, Mingo N and ShengBTE N 2014 A solver of the Boltzmann transport equation for phonons *Comput. Phys. Commun.* **185** 1747–58

[36] Togo A, Oba F and Tanaka I 2008 First-principles calculations of the ferroelastic transition between rutile-type andCaCl2-typeSiO2at high pressures *Phys. Rev.* B **78** 134106

[37] Ouyang T and Hu M 2015 Competing mechanism driving diverse pressure dependence of thermal conductivity of *X*Te (X=Hg, Cd, and Zn) *Phys. Rev.* B **92** 235204

[38] Qin G, Qin Z, Wang H and Hu M 2017 Anomalously temperature-dependent thermal conductivity of monolayer GaN with large deviations from the traditional 1/*T* law *Phys. Rev.* B **95** 195416

[39] Yue S-Y, Zhang X, Qin G, Yang J and Hu M 2016 Insight into the collective vibrational modes driving ultralow thermal conductivity of perovskite solar cells *Phys. Rev.* B **94** 115427

[40] Yang J-Y, Qin G and Hu M 2016 Nontrivial contribution of Fröhlich electron-phonon interaction to lattice thermal conductivity of wurtzite GaN *Appl. Phys. Lett.* **109** 242103

[41] Ouyang T, Xiao H, Tang C, Zhang X, Hu M and Zhong J 2016 First-principles study of thermal transport in nitrogenated holey graphene *Nanotechnology* **28** 045709

[42] Yue S-Y, Ouyang T and Hu M 2015 Diameter dependence of lattice thermal conductivity of single-walled carbon nanotubes: study from Ab Initio *Sci. Rep.* **5** 15440

[43] Yue S-Y, Qin G, Zhang X, Sheng X, Su G and Hu M 2017 Thermal transport in novel carbon allotropes with sp^2 or sp^3 hybridization: an ab initio study *Phys. Rev.* B **95** 085207

[44] Ouyang T, Xiao H, Tang C, Hu M and Zhong J 2016 Anisotropic thermal transport in Weyl semimetal TaAs: a first principles calculation *Phys. Chem. Chem. Phys.* **18** 16709–14

[45] Wang H, Qin G, Li G, Wang Q and Hu M 2017 Low thermal conductivity of monolayer ZnO and its anomalous temperature dependence *Phys. Chem. Chem. Phys.* **19** 12882

[46] Qin G, Qin Z, Wang H and Hu M 2018 Lone-pair electrons induced anomalous enhancement of thermal transport in strained planar two-dimensional materials *Nano Energy* **50** 425–30

[47] Qin G, Qin Z, Wang H and Hu M 2018 On the diversity in the thermal transport properties of graphene: a first-principles-benchmark study testing different exchange-correlation functionals *Comput. Mater. Sci.* **151** 153–9
[48] Lee S, Esfarjani K, Luo T, Zhou J, Tian Z and Chen G 2014 Resonant bonding leads to low lattice thermal conductivity *Nat. Commun.* **5** 3525
[49] Slack G A 1973 Nonmetallic crystals with high thermal conductivity *J. Phys. Chem. Solids* **34** 321–35
[50] Li W and Mingo N 2014 Lattice dynamics and thermal conductivity of skutterudites $CoSb_3$ and $IrSb_3$ from first principles: why $IrSb_3$ is a better thermal conductor than $CoSb_3$ *Phys. Rev.* B **90** 094302
[51] Lindsay L 2016 First principles peierls-boltzmann phonon thermal transport: a topical review *Nanoscale and Microscale Thermophysical Eng.* **20** 67–84
[52] Qi J *et al* 2010 Ultrafast carrier and phonon dynamics in Bi2Se3 crystals *Appl. Phys. Lett.* **97** 182102
[53] Lindsay L and Broido D A 2008 Three-phonon phase space and lattice thermal conductivity in semiconductors *J. Phys.: Condens. Matter* **20** 165209
[54] Okubo K and Tamura S-I 1983 Two-phonon density of states and anharmonic decay of large-wave-vector LA phonons *Phys. Rev.* B **28** 4847–50
[55] Peng B, Zhang H, Shao H, Xu Y, Zhang X and Zhu H 2016 Low lattice thermal conductivity of stanene *Sci. Rep.* **6** 20225
[56] Lindsay L, Broido D A, Carrete J, Mingo N and Reinecke T L 2015 Anomalous pressure dependence of thermal conductivities of large mass ratio compounds *Phys. Rev.* B **91** 121202
[57] Mukhopadhyay S and Stewart D A 2014 Polar effects on the thermal conductivity of cubic boron nitride under pressure *Phys. Rev. Lett.* **113** 025901
[58] Karki B B and Wentzcovitch R M 2003 Vibrational and quasiharmonic thermal properties of CaO under pressure *Phys. Rev.* B **68** 224304